Heliyon 8 (2022) e11353

Contents lists available at ScienceDirect

Heliyon

journal homepage: www.cell.com/heliyon

Research article

Analysis of performance, emissions, and lubrication in a spark-ignition engine fueled with hydrogen gas mixtures

Carlos Pardo García [a], Sofia Orjuela Abril [b,*], Jhon Pabón León [b]

[a] Programa de Ingeniería de Sistemas, Universidad Francisco de Paula Santander, Avenida Gran Colombia No. 12E-96 Barrio Colsag, San José de Cúcuta 540001, Colombia

[b] Programa de Administración de Empresas, Universidad Francisco de Paula Santander, Avenida Gran Colombia No. 12E-96 Barrio Colsag, San José de Cúcuta 540001, Colombia

ARTICLE INFO

Keywords:
Spark ignition engine
Hydrogen gas
Lubricating oil
Emissions
Performance

ABSTRACT

Hydrogen is one of the main alternative fuels with the greatest potential to replace fossil fuels due to its renewable and environmentally friendly nature. Due to this, the present investigation aims to evaluate the combustion characteristics, performance parameters, emissions, and variations in the characteristics of the lubricating oil. The investigation was conducted in a spark-ignition engine fueled by gasoline and hydrogen gas. Four engine load conditions (25%, 50%, 75%, and 100%) and three hydrogen gas mass concentration conditions (3%, 6%, and 9%) were defined for the study. The investigation results allowed to demonstrate that the injection of hydrogen gas in the gasoline engine causes an increase of 3.2% and 4.0% in the maximum values of combustion pressure and heat release rates. Additionally, hydrogen causes a 2.9% increase in engine BTE. Hydrogen's more efficient combustion process allowed for reducing CO, HC, and smoke opacity emissions. However, hydrogen gas causes an additional increase of 14.5% and 30.4% in reducing the kinematic viscosity and the total base number of the lubricating oil. In addition, there was evidence of an increase in the concentration of wear debris, such as Fe and Cu, which implies higher rates of wear in the engine's internal components.

1. Introduction

Fossil fuels are one of the main fuels source used in different economic sectors, such as the transport, industrial, agricultural, and power generation sectors. This has led to an accelerated consumption of fossil resource reserves and an increase in oil prices. Additionally, the use of fuels produces polluting emissions, which are responsible for global warming and climate change [1]. Due to this situation, it is necessary to search for new strategies, technologies, and alternative fuels to reduce the consumption of fossil fuels such as gasoline [2]. This satisfies the fuel demand and guarantees environmental safety [3].

To overcome the problem of scarcity of fossil resources and environmental pollution, technologies based on the electrification of propulsion systems have been proposed [4]. This involves the use of electric and hybrid vehicles, such as battery electric vehicles (BEV), hybrid electric vehicles (HEV), and fuel cell hydroelectric vehicles (FCHEV). Despite the environmental benefits of this type of technology, it is still necessary to overcome various challenges related to the weight of the batteries, the high economic cost, the high demand for lithium, and environmental concerns associated with mining activities. Therefore, the complete replacement of internal combustion engines is gradual, especially in developing countries. This situation implies that internal combustion engines (ICE) still have a long life in the industrial and transport sectors [5]. Since that electrification is not an immediate solution to solve energy demand and environmental problems, it is necessary to consider alternatives such as dual-fuel systems. Auxiliary fuel injection is an alternative to reduce fuel consumption and improve polluting emission levels [6].

Alternative fuel research in gasoline engines focuses on using green fuels to reduce the carbon footprint [7]. Studies indicate that dual-fuel engines have reduced emissions compared to pure gasoline [8]. Currently, among the most used alternative fuels in gasoline engines are compressed natural gas (CNG), ethanol, and liquefied petroleum gas (LPG), among others [9, 10, 11, 12, 13]. This is due to the closeness of the physicochemical properties compared to gasoline. Additionally, they require minor modifications and are environmentally friendly [14]. However, the results of the investigations indicate a reduction in power performance when using this type of alternative fuel [15].

* Corresponding author.
E-mail address: sofiaorjuela@ufps.edu.co (S. Orjuela Abril).

https://doi.org/10.1016/j.heliyon.2022.e11353
Received 8 May 2022; Received in revised form 7 June 2022; Accepted 26 October 2022

Hydrogen has been considered one of the most promising alternative fuels due to its ability to reduce exhaust gas emissions without affecting performance in gasoline engines [16, 17]. The investigations carried out indicate that hydrogen, in combination with gasoline, is an adequate method to improve fuel economy and reduce polluting gases. Additionally, hydrogen is considered an inexhaustible fuel and has the ability to be produced from processes such as water electrolysis [18]. Another advantage of hydrogen is the improvement in the engine's useful life due to the decrease in the percentage of carbon deposits. El-Kassaby [19] reported that hydrogen injection caused a 10% increase in the engine's thermal efficiency. Additionally, a reduction of 34%, 18%, and 15% in CO, HC, and NOx emissions was observed compared to the engine running without hydrogen injection. Castro et al. [20] indicated a reduction in the specific diesel consumption by hydrogen addition. Karagoz et al. [21] demonstrated that hydrogen allows for minimizing HC and CO emissions. Tutak et al. [22] indicated that the mixture of hydrogen and natural gas caused a reduction in the duration of combustion and a shortening of the time of achieving, compared to the engine without hydrogen. Ebrahimi and Jazayeri [23] reported a reduction in CO emissions and a decrease in fuel consumption compared to the engine running without hydrogen injection. Zareei et al. [24] showed that the brake thermal efficiency of the engine increased in HCNG (hydrogen - compressed natural gas) blends compared to pure diesel and CNG. Atul Dhar et al. [25] investigated the performance of an internal combustion engine when fueled with pure diesel and biodiesel blend (B20) from Karanja oil. The study focused on analyzing the tribological characteristics of the lubricating oil. The results showed an increase in wear and higher ash and soot content in the engine during operation with biodiesel compared to diesel. Murugan et al. [26] studied the effect of using tire pyrolysis oil in an engine during a 100-hour test. Reports indicated an increase in wear residues in the lubricating oil. Zare et al. [27] investigated the change in NOx emissions when used lubricating oil is used as a fuel additive. The investigation showed that the use of waste lubricating oil causes a decrease in NOx emissions.

Asrar et al. [28] evaluated the impact of n-butanol blends on engine lubricating oil degradation in a gasoline engine. The results indicated that the development of lubricating oil is necessary to improve its life cycle. Usman et al. [29] investigated the effect of compressed natural gas on the deterioration of lubricating oil. From the results, a higher metal concentration was evidenced than pure gasoline. Similarly, Yan et al. [30] studied the performance and emissions of an engine fueled with hydrogen and natural gas mixtures. It was found that hydrogen enrichment in natural gas could reduce HC, CO_2, and CO emissions. Usman et al. [31] evaluated engine performance and lubricating oil deterioration with liquid and gaseous engines. Significant improvement was observed for wear debris, lube oil physicochemical characteristics, and additive depletion for CNG. Mathai et al. [32] studied the performance, emission, lubricant, and reservoir characteristics of a spark-ignition engine fueled by compressed natural gas and hydrogen. During the tests, it was reported that the kinematic viscosity decreases significantly with the hydrogen and natural gas mixtures. Usman et al. [33] investigated the regeneration of deteriorated oil and the impact of reclaimed oil on engine performance and engine emissions. Regeneration has improved oil properties and positively impacted engine performance and emissions.

The research mentioned above demonstrates the potential of hydrogen to improve performance and minimize the environmental impact of internal combustion engines. However, the analysis of lubricating oil conditions has been little addressed, especially in gasoline engines. The composition of the lubricating oil and the operating conditions affect the engine's fuel consumption [34]. Additionally, by-products from lubricating oil deterioration have an adverse effect on the environment and human health. This is a consequence of the oxidation of light materials such as alcohols, acids, and ketones [35]. Since the fuel type affects the quality of the lubricating oil, it is necessary to evaluate the impact of alternative fuels on the lubrication characteristics of the engine.

Due to the above, this research aims to evaluate the combustion characteristics, performance parameters, emissions, and variations in the physicochemical properties of lubricating oil in spark-ignition engines fueled with gasoline and hydrogen gas mixture.

2. Materials and methods

2.1. Experimental setup

For the research development, a spark-ignition engine was used, with a compression ratio of 8.5:1, displacement of 171 cm^3, and natural aspiration. The injection system consists of a carburetor, which allows you to control the amount of fuel. Additionally, an air-hydrogen mixer was used in the engine intake. The main characteristics of the engine are described in Table 1.

Figure 1 illustrates the scheme of the experimental test bench, which is formed by the gasoline engine test bench and the hydrogen generation bench.

The control of the load conditions and rotation speed in the test engine was carried out by means of a resistive load bank. A piezoelectric transducer type cooled sensor (KISTLER type 7063-A) was installed in the engine cylinder to measure the pressure in the combustion chamber. The piezoelectric transducer was located flush with the cylinder head. A data filtering process was carried out during all the recorded cycles to eliminate high-frequency oscillations to treat the pressure signals. The applied filter consists of transforming the discretized signal from the time domain to the frequency domain. A crank angle sensor (Beck Arnley 180–042) was used for rotational speed measurement. A hot wire type mass airflow sensor (BOSCH 22680-7J600) was installed to measure intake air flow. The fuel consumption measurement was calculated by using a precision balance (OHAUS PA313) and a stopwatch. The temperature of the exhaust gases and the interior of the combustion chamber were measured using type K thermocouple sensors. To synchronize the pressure data, a capacitive TDC sensor was used.

A gas analyzer (BrainBee AGS-688) was used to analyze polluting emissions from combustion gases. Additionally, an opacimeter (BrainBee OPA-100) was used to measure the opacity levels of smoke emissions. The characteristics of the instruments used to analyze the emissions are shown in Table 2.

The characteristics of the engine bench measuring instruments are shown in Table 3.

The hydrogen generation bench was installed in the engine's air intake system. The generation of hydrogen was carried out by means of a water electrolysis process. The chemical reaction present at the electrodes is shown in Eqs. (1) and (2) [36].

Cathode (reduction):

$$2H_2O_{(l)} + 2e^- \rightarrow H_{2(g)} + 2OH^-_{(aq)} \quad (1)$$

Anode (oxidation):

$$4OH^-_{(aq)} \rightarrow O_{2(g)} + 2H_2O_{(l)} + 4e^- \quad (2)$$

Table 1. Characteristics of the gasoline engine.

Specification	Value	Unit
Model	4T OHV	-
Displacement	171	cm^3
Bore	66	mm
Stroke	50	mm
Fuel capacity	4.5	L
Maximum power	3.5	kW
Ignition system	Transistor Controlled Igniter	-
Compression ratio	8.5/1	-
Maximum torque	10.5 @ 2400 rpm	Nm

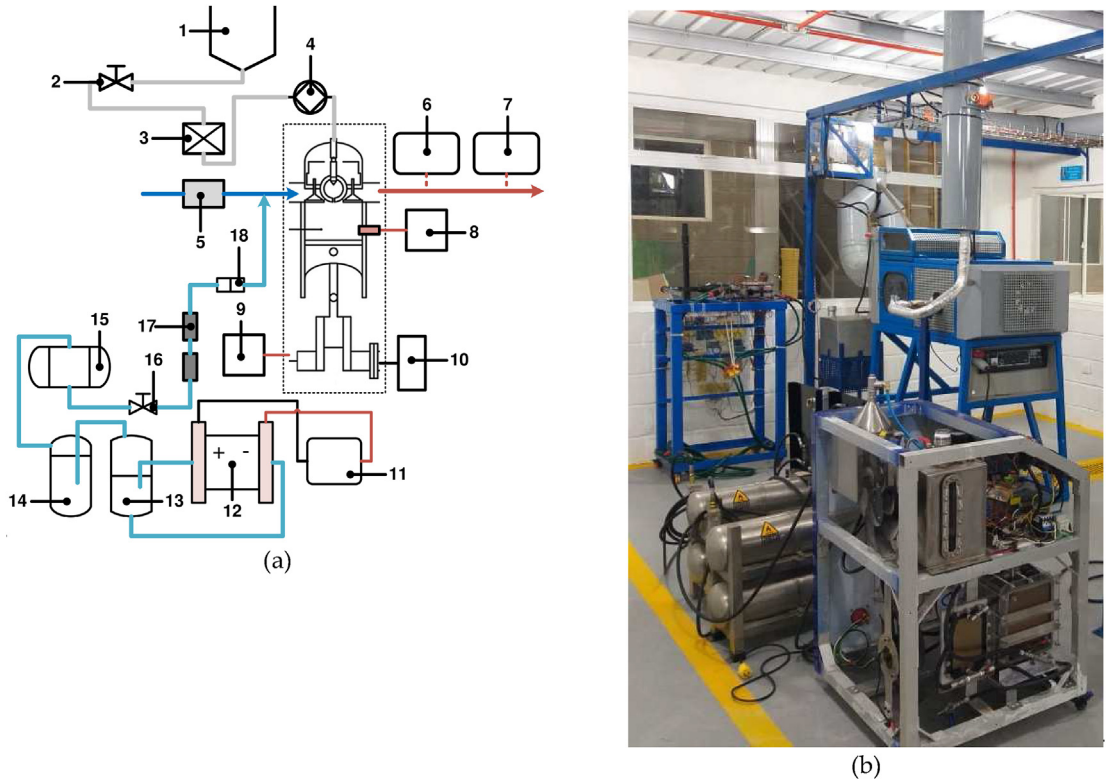

Figure 1. Engine test bench (a) diagram and (b) test bench. 1. Gravimetric fuel meter, 2. Fuel inlet valve, 3. Fuel filter, 4. Injection pump, 5. Air flow meter, 6. BrainBee AGS-688, 7. BrainBee OPA-100, 8. In-cylinder pressure, 9. Encoder, 10. Load bank, 11. AC – DC converter, 12. Dry cell, 13. Electrolytic tank, 14. Bubbler, 15. Storage tank, 16. Hydrogen gas flow meter, 17. Flame arrester, 18. Silica gel filter.

Table 2. Characteristics of exhaust gas analyzers.

Manufacturer	Instrument	Parameter	Range	Resolution	Uncertainty
BrainBee AGS-688	Exhaust gas analyzer	CO	0–9.99% vol.	0.01	± 0.01%
		CO_2	0–19.9% vol.	0.1	± 0.1%
		HC	0–9999 ppm vol.	1	± 1%
		NOx	0–5000 ppm vol.	1	± 1%
BrainBee OPA-100	Opacimeter	Smoke opacity	0–99%	0.1	± 0.1%

Table 3. Engine bench measuring instruments.

Manufacturer	Instrument	Parameter	Range	Uncertainty
KISTLER type 7063-A	Piezoelectric transducer	Cylinder pressure	0–250 bar	± 0.25%
OHAUS-PA313	Precision balance	Fuel measuring	0–310 g	± 0.5%
BOSCH 22680-7J600	Air mass sensor	Airflow	0–125 g/s	±1%
Beck Arnley 180-042	Crankshaft angle	Angle	5–9999 rpm	± 0.2%
Type K	Temperature sensor	Temperature	-200–1370 °C	± 0.7%
Masterflex	Flowmeter	Volumetric flow gas hydrogen	0.01–1 LPM	± 0.25%

The bench is made up of an electrolytic tank and a bubbler, which allow a continuous flow of water to be maintained in the dry cell and trap the water vapor mixed with the hydrogen gas. The above is in order to prevent the entry of water into the chamber of the engine. The dry cell was built using stainless steel plates due to its high conductivity, high corrosion resistance, temperature resistance, and voltage resistance.

Table 4. Properties of hydrogen gas.

Property	Value	Unit
Chemical formula	H_2	[-]
Density	0.08376	kg/m^3
Lower heat value	120.21	MJ/kg
Molecular weight	2.01594	kg/kmol

Additionally, stainless steel is compatible with a wide variety of electrolytic substances. The dimensions of the steel plates are 20 cm (height), 13.3 cm (width), and 0.15 cm (thickness). A separation distance of 2 mm was established between each of the plates. KOH was used as a catalyst with a concentration of 20% due to its high conductivity. The generated hydrogen gas is stored in storage tanks, which were designed taking as reference the ASME Code Section VIII Division 1 for pressure vessels [37]. The construction material of the tanks was 304 austenitic stainless steel. As for safety measures, a silica gel filter and two flame arresters were installed to prevent the flame's flashback towards the hydrogen generation system. The physicochemical characteristics of hydrogen gas are shown in Table 4.

2.2. Experimental procedure

Experimental tests were performed at a constant rotation speed of 1500 rpm since the gasoline engine is mainly used to generate electrical energy. Therefore, it is necessary to maintain a fixed operating frequency. To consider the different operating conditions of the engine, four load levels were selected (25%, 50%, 75%, and 100%). The four engine load conditions are equivalent to a brake mean effective pressure of 2 bar (25%), 4 bar (50%), 6 bar (75%), and 8 bar (100%), respectively.

The engine intake air flow was varied from 30:1 to 45:1, where 45:1 corresponds to the lowest load and 30:1 to the highest engine load. For the development of the study, the ignition angle was kept constant. For each engine load condition, three levels of hydrogen gas mass concentration (3%, 6%, and 9%) were evaluated. The hydrogen injection was carried out through a Venturi injector in the engine intake air system to obtain a mixture of air + hydrogen that entered the combustion chamber. Hydrogen was injected at a constant pressure of 4 bar during all the experimental tests.

The measurement and recording of the measured parameters were carried out after reaching a stable condition in the engine. Additionally, the experimental tests were repeated five times to guarantee the results' reliability without causing an excessively long test time. The amount of fuel was adjusted by a control valve at the fuel supply inlet. For the development of the experimental tests, the ignition angle was kept constant. The spark-ignition engine was fueled with gasoline, whose physicochemical properties are illustrated in Table 5.

For the study of the characteristics and deterioration of the lubricating oil, the engine operated for 150 h, in which samples were collected every 25 h. The foregoing was defined, taking into consideration the recommendations described in the literature [31, 38]. After each test, the lubricating oil was drained and filled with fresh lubricating oil. The standards used to determine the viscosity, flash point, TAN, and TBN characteristics of the lubricating oil are indicated in Table 6. The kinematic viscosity was measured using a viscometer. The measurement of metal concentrations was performed using a multi-element ICP-MS analyzer. The properties of the lubricating oil used in the experimental tests are indicated in Table 6.

The composition of the fuels used in the experimental tests is described in Table 7. The amount of intake air was regulated by means of a control valve in order to keep the lambda parameter constant regardless of the percentage of hydrogen substitution. Additionally, the amount of fuel (gasoline) was regulated by means of a control valve to maintain equivalence in mass concerning the amount of hydrogen injected into the engine. The regulation of the fuel, hydrogen gas, and intake air flow allows the engine to run with a stoichiometric mixture at different load percentages. The foregoing is to be able to make an adequate comparison between the different fuel mixtures.

The equations used for the conversion of exhaust gas emissions are shown below [39].

$$CO\ (g/kWh) = 3.591 \times 10^{-3} \times CO\ (ppm) \tag{3}$$

$$NO_x\ (g/kWh) = 6.636 \times 10^{-3} \times NO_x\ (ppm) \tag{4}$$

Table 5. Physicochemical properties of gasoline.

Property	Value	Unit
Density	737	kg/m^3
Laminar flame speed	33	cm/s
Lower heat value (LHV)	43.4	MJ/kg
Autoignition temperature	300	°C
Vaporization latent heat	440	kJ/kg

Table 6. Physicochemical properties of lubricating oil.

Property	ASTM Method	Value	Unit
Grade	SAE J300	SAE 15W40	[-]
TAN	D664	1.8	mg-KOH/g
Flash point	D-92	226	°C
TBN	D-2896	5.2	mg-KOH/g
Kinematic viscosity @ 40 °C	D-445	105.4	cSt
Kinematic viscosity @ 100 °C	D-445	14.18	cSt

$$HC\ (g/kWh) = 2.002 \times 10^{-3} \times HC\ (ppm) \tag{5}$$

3. Combustion model

The ideal gas state formula was used to calculate the instantaneous temperature inside the combustion chamber with respect to the crankshaft angle, which is indicated in Eq. (6) [40].

$$T_g = \frac{P \times V}{m_c \times R} \tag{6}$$

where P is the in-cylinder pressure, V is the instantaneous in-cylinder volume, m_c is the in-cylinder mass, and R is the gas constant, respectively.

To calculate the instantaneous in-cylinder volume, the variations caused by the chamber's deformations and clearances were considered, as indicated in Eq. (7) [41].

$$V = V_m + V_c + \Delta V_p + \Delta V_{inertial} + \Delta V_{clearance} \tag{7}$$

where V_m is the volume of the free space when the piston reaches top dead center (TDC), V_c is the volume displaced due to the connecting rod-crank mechanism, ΔV_p is the volumetric strain caused by pressure, $\Delta V_{inertial}$ do the inertial forces and induce the volumetric strain $\Delta V_{clearance}$ do the clearances cause the volume in the combustion chamber. The previous volume variations were considered due to their influence on the instantaneous volume, which causes significant changes in the prediction of the thermodynamic behavior of the engine [41]. The calculation of each of the terms of Eq. (7) is shown below [41, 42]:

$$V_m = \frac{\pi D^2 l_c}{2(r_c - 1)} \tag{8}$$

$$V_c = \frac{\pi D^2 (l_c + l_r - r_y)}{4} \tag{9}$$

$$\Delta V_p = \frac{\pi D^2 l_r A_p k_d P}{4 E_s A_c} \tag{10}$$

$$\Delta V_{inertial} = \frac{\pi D^2 l_r k_d a_p m_c}{4 E_s A_c} \tag{11}$$

$$\Delta V_{clearance} = \frac{\pi D^2}{4} \sum_{i=1}^{2} (e_i \sin \varphi_i \cos \alpha_i) \tag{12}$$

where D is the internal diameter of the piston, l_r is the length of the connecting rod, l_c is the crankshaft length, r_c is the compression ratio, r_y

Table 7. Experimental test fuel blends.

Nomenclature	Composition
G100	Gasoline
G100 + 3% H_2	Gasoline + hydrogen mass fraction 3%
G100 + 6% H_2	Gasoline + hydrogen mass fraction 6%
G100 + 9% H_2	Gasoline + hydrogen mass fraction 9%

Table 8. Modified Woschni correlation C_1 and C_2 value [45].

Phase	C_1	C_2
Intake	309/50	0
Compression	57/25	0
Combustion	57/25	0.00324
Expansion	57/25	0.00324
Exhaust	309/50	0

is the vertical position of the piston, A_p is the piston cross-sectional area, k_d is the deformation, E_s is the elastic modulus of steel, A_c is the piston cross-sectional area and a_p is the piston acceleration, φ is the angle of rotation, and α is the between the piston and connecting rod, respectively.

The heat release rate (HHR) was calculated from the first law of thermodynamics, instantaneous volume data, and the pressure in the combustion chamber. The heat release rate by the combustion process with respect to the crank angle was determined from Eq. (13) [43].

$$\frac{dQ}{d\theta} = \frac{1}{\gamma - 1} \times \left(\gamma P \frac{dV}{d\theta} + V \frac{dP}{d\theta} \right) + \frac{dQ_{loss}}{d\theta} \tag{13}$$

where γ is the specific heat ratio of in-cylinder gas and Q_{loss} is the heat loss from the engine cylinder. To calculate the heat loss, Eq. (14) was used [43].

$$\frac{dQ_{loss}}{d\theta} = h_c \times A_c \times \frac{d(T_g - T_w)}{d\theta} \tag{14}$$

where T_g is the temperature of the cylinder wall, A_c is the instanteneous surface area of the combustion chamber and h_c is the heat transfer coefficient. The heat transfer coefficient was calculated using the modified Woschni correlation to consider the effects of hydrogen addition. Eq. (15) expresses the calculation of the heat transfer coefficient [44].

$$h_c = 129.9 \times d^{-0.2} \times P^{0.8} \times T_g^{-0.53} \times \left(C_1 \times C_m + C_2 \times \frac{V_s \times T_r}{P_r \times V_r} \times (P - P_m) \right)^{0.8} \tag{15}$$

where d is the cylinder bore diameter, C_m is the mean piston velocity, V_s is the clearance volume of the combustion chamber, P_r and V_r are the reference pressure and volume, respectively. The reference was considered to be the inlet valve closing (IVC). C_1 and C_2 are model constants whose values depend on the stage of the combustion cycle. The values used are shown in Table 8.

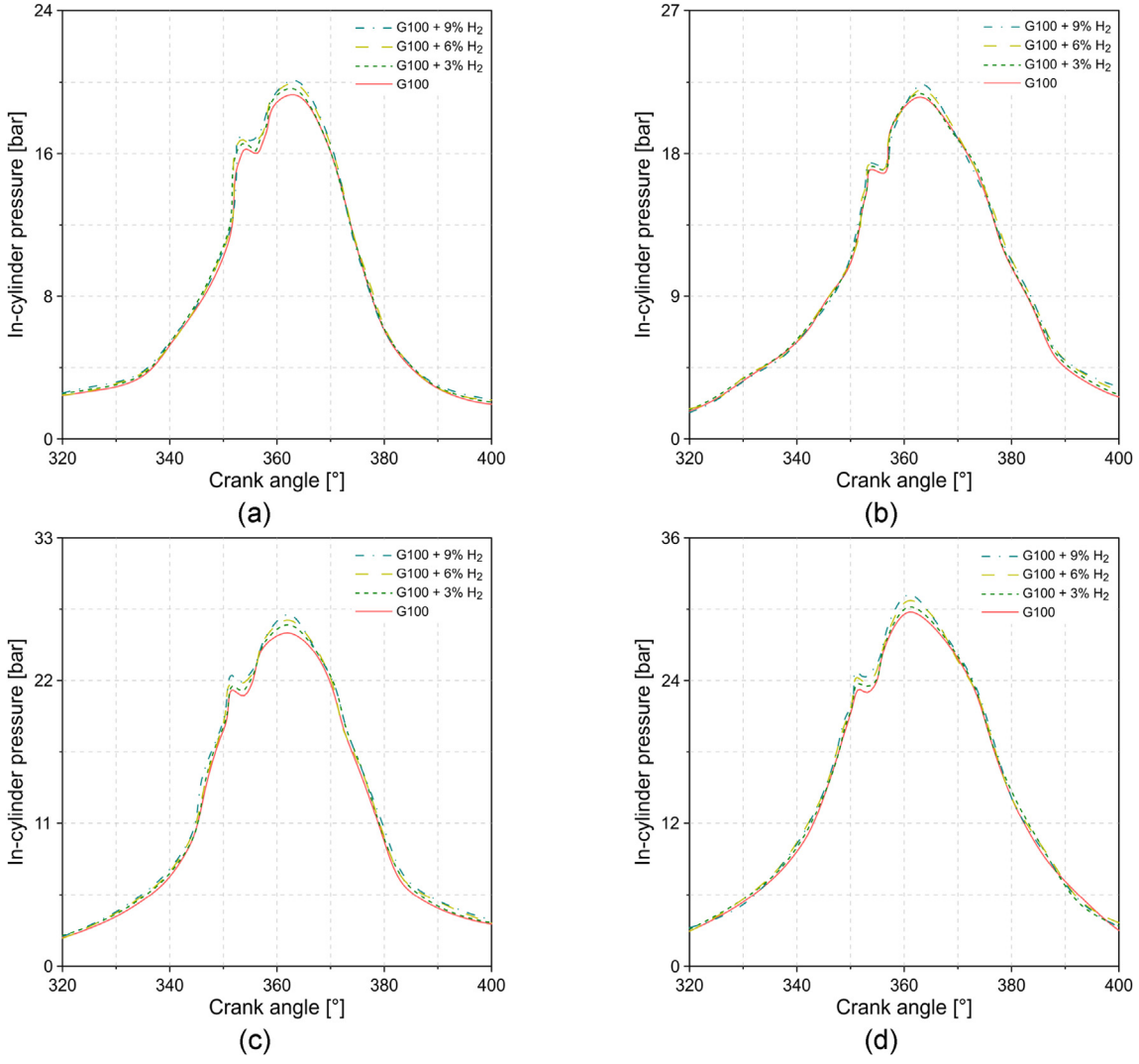

Figure 2. Pressure curves in the combustion chamber for a load of (a) 25%, (b) 50%, (c) 75% and 100% (d).

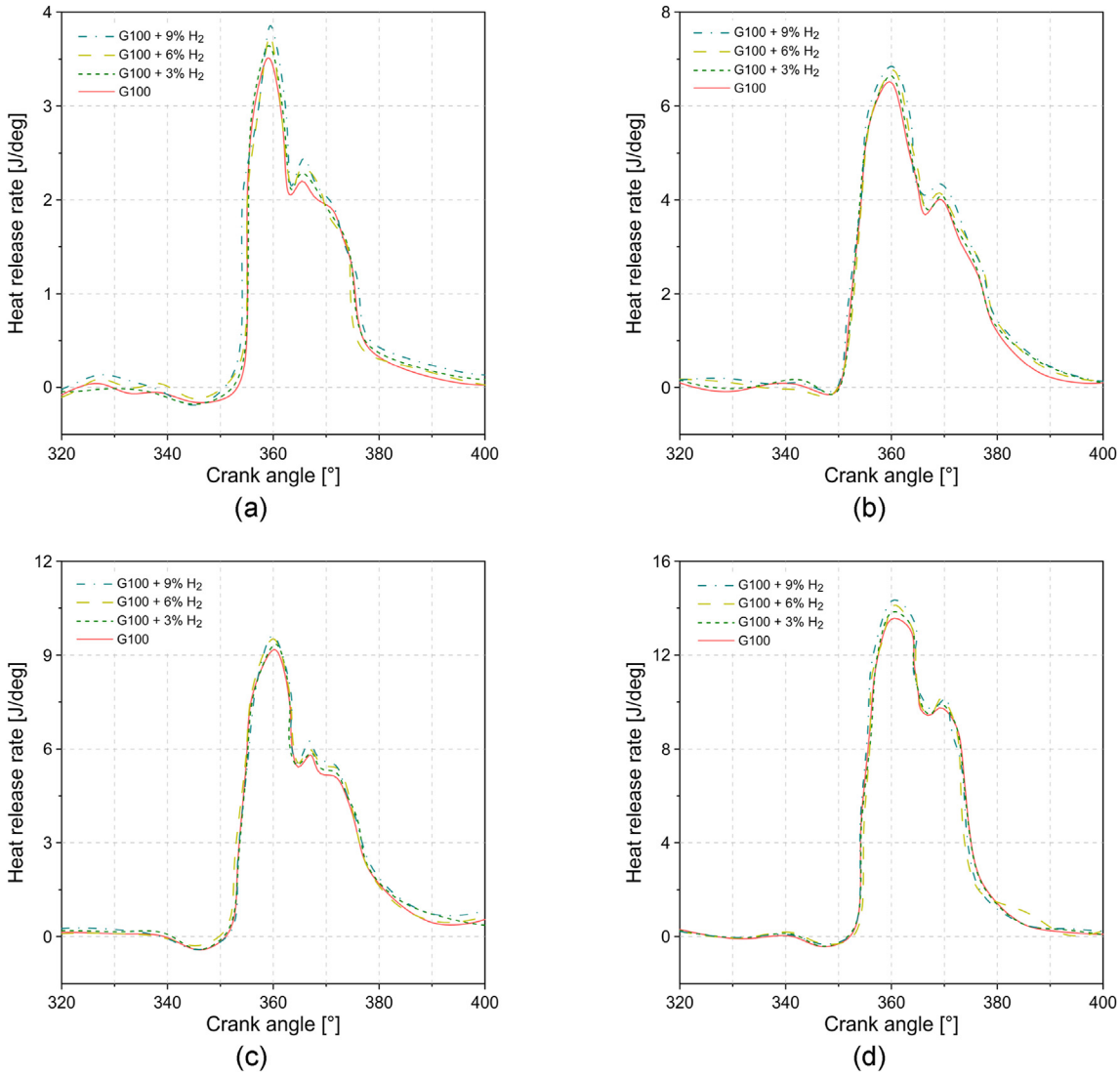

Figure 3. Heat release rate for a load of (a) 25%, (b) 50%, (c) 75% and (d) 100%.

The mass fraction burned (MFB) was calculated using the method proposed by Rassweiler and Withrow [46], as shown in Eq. (16).

$$MFB = \frac{m_{q(i)}}{m_{q(t)}} = \frac{\sum_0^i dP_c}{\sum_0^i dP} \tag{16}$$

where dP is the in-cylinder pressure variation and dP_c is the pressure variation caused by the combustion process. The pressure change caused by volume reduction (dP_v) was calculated from Eqs. (17) and (18) [47].

$$\Delta P = \Delta P_v + \Delta P_c \tag{17}$$

$$\Delta P_v = P_\theta \times \left[\left(\frac{V_{\theta+1}}{V_\theta}\right)^\gamma - 1\right] \tag{18}$$

4. Results and discussion

4.1. Combustion characteristics

Figures 2(a–d) shows the pressure curves of the combustion chamber for the different load conditions and hydrogen gas injection flow.

From the results described in Figure 2, it was evidenced a maximum pressure for 100% load of 29.7 bar, 30.1 bar, 30.7 bar and 31.2 bar with fuel G100, G100 + 3% H_2, G100 + 6% H_2 and G100 + 9% H_2, respectively (see Figure 2d). In general, the pressure curves show a growth when the engine load is increased, which is attributed to the greater injection of fuel to meet the power demand. Additionally, the injection of hydrogen gas allowed for increasing the maximum pressure of the combustion chamber. This is attributed to the increase in pressure and the hydrogen flame's high velocity since it favors the combustion process. The behavior obtained is in agreement with the findings in the literature for other types of fuels [46]. For the tested conditions, an increase in the maximum pressure of 1.4%, 3.2%, and 4.9% was obtained with an injection of hydrogen gas from 3% H_2, 6% H_2, and 9% H_2, respectively. In general, it is observed that in all the pressure curves, two peaks are produced, which are associated with the compression stage (first peak) and the expansion stage (second peak). The behavior of the pressure curves is mainly related to the fuel injection time. Similar trends are reported in the literature [48, 49, 50].

The behavior of the heat release rate is indicated in Figures 3(a–d).

The heat release rate is an indication of the amount of chemical energy that can be transformed into thermal energy. The addition of hydrogen gas in gasoline causes an increase in the HRR of the engine. The addition of hydrogen gas at 3% H_2, 6% H_2, and 9% H_2 allowed an increase of 2.1%, 4.1%, and 5.8%% in the maximum heat release rate compared to pure gasoline at 100% load, respectively. The increase of

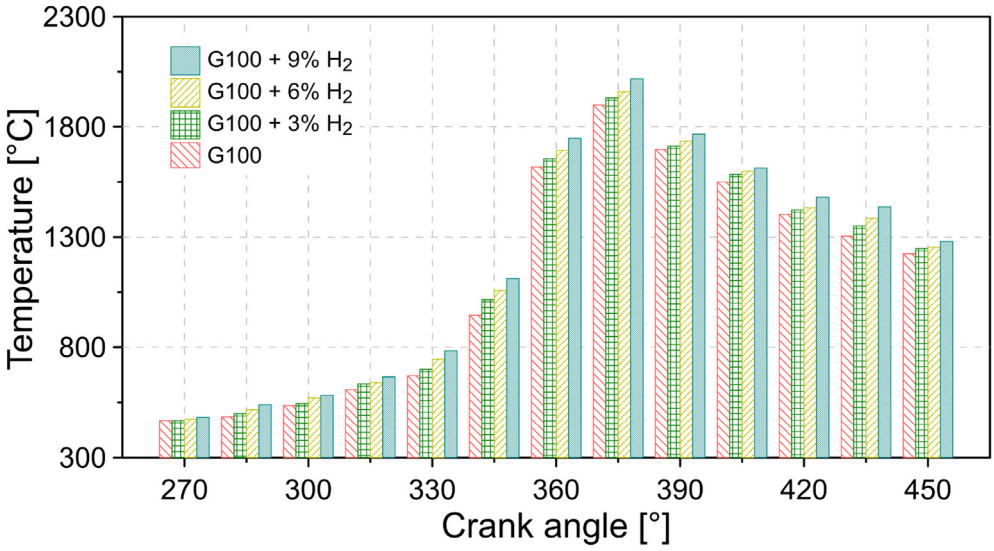

Figure 4. Average combustion temperature for 100% load.

heat release rate due to hydrogen injection can be attributed to better diffusion of the fuel mixture and the rapid heat release from hydrogen combustion. Additionally, hydrogen has a significantly higher lower heat value compared to gasoline, which is another variable that contributes to the increase in engine HRR. Similar to the results in Figure 2, the heat release rate curves have two peaks corresponding to the premixed combustion phase (first peak) and the diffusion phase (second peak), respectively.

Figure 4 shows the average temperature levels of the combustion chamber for the different flow conditions of hydrogen gas in the engine.

In general, the temperature of the combustion increases with the addition of hydrogen gas. For the tested condition, a maximum temperature of 1900 °C, 1931 °C, 1960 °C and 2018 °C was obtained with fuel G100, G100 + 3% H_2, G100 + 6% H_2 and G100 + 9% H_2, respectively. On average, the injection of 3% H_2, 6% H_2, and 9% H_2 into the engine causes a 2.7%, 5.1%, and 8.4% increase in combustion temperature compared to gasoline. This behavior is a consequence of the higher release rates, as shown in Figure 3, and the high calorific value of hydrogen. Hora and Agarwal [51] reported similar trends in mean combustion gas temperature with the addition of hydrogen in an engine fueled by compressed natural gas.

4.2. Performance characteristics

To evaluate the performance of the engine in the different combustion conditions, the trend of the brake specific fuel consumption (BSFC) was analyzed under a load of 25%, 50%, 75%, and 100%, respectively. The BSFC was calculated from Eq. (19).

$$BSFC = \frac{\dot{m}_g + \left(\dot{m}_h \times \frac{LHV_h}{LHV_g}\right)}{\dot{W}_{engine}} \tag{19}$$

where $\dot{m}_g$ gasoline mass flow rate, $\dot{m}_h$ hydrogen mass flow rate, LHV_h is the lower heat value of hydrogen, LHV_g is the lower heat value of gasoline and $\dot{W}_{engine}$ engine power output, respectively. The results obtained are shown in Figure 5.

In general, the higher calorific value present in hydrogen gas caused a reduction in the BSFC of the engine, which indicates a reduction in fuel consumption. Additionally, the high degree of flammability of hydrogen contributes to improving the combustion process. The gaseous characteristic of hydrogen and the high autoignition temperature facilitates its mixing with air and allows the engine to run with lean mixtures [52]. The

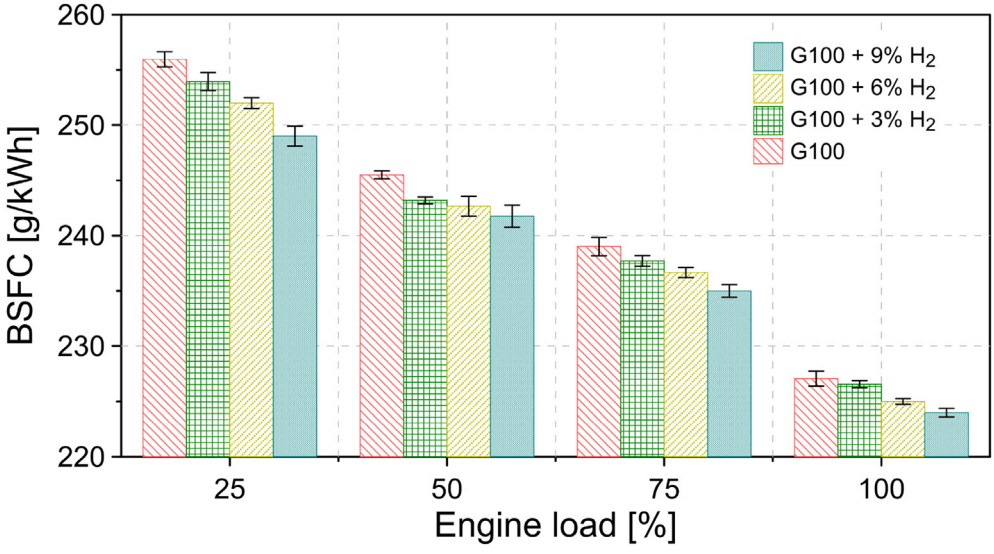

Figure 5. Brake specific fuel consumption of the engine for different load conditions.

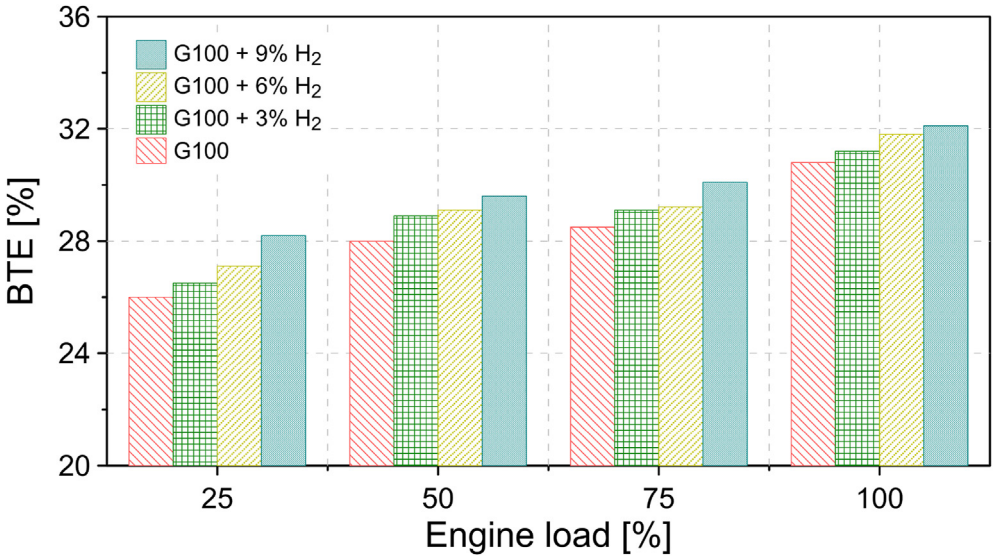

Figure 6. Brake thermal efficiency of the engine for different load conditions.

addition of a hydrogen gas flow of 3% H_2, 6% H_2, and 9% H_2 in the engine caused a decrease in BSFC of 0.6%, 1.2%, and 1.8% compared to pure gasoline. Additionally, it is evident that the increase in load tends to reduce the BSFC of the engine, which implies a reduction in fuel consumption for higher loads. In the case of a 25% load, a value of 256 g/kWh, 254 g/kWh, 252 g/kWh and 249 g/kWh were obtained for fuels G100, G100 + 3% H_2, G100 + 6% H_2 and G100 + 9% H_2, respectively. However, for a 100% load on the engine, values of 227.1 g/kWh, 226.6 g/kWh, 225 g/kWh, and 223 g/kWh were found.

Figure 6 shows the effect of hydrogen on the brake thermal efficiency (BTE) for different engine load conditions.

In general, it was observed that the thermal efficiency of the engine increased with the mixture of gasoline and hydrogen gas. This improvement in engine efficiency is directly associated with the reduction in gasoline consumption, as indicated in Figure 5. The engine's brake thermal efficiency is highly dependent on combustion performance, which deteriorates significantly at low load levels. Due to the above, the improvement in the BTE of the engine operating with hydrogen mixtures was more evident for a load of 25%. Similar trends are reported in the literature [53]. The highest BTE values are obtained at maximum engine load, whose values were 30.8%, 31.2 %, 31.8% and 32.1% for fuels G100, G100 + 3% H_2, G100 + 6% H_2 and G100 + 9% H_2, respectively.

4.3. Emissions characteristics

The CO emissions of the engine for the different load conditions are described in Figure 7.

The formation of carbon monoxide occurs due to the incomplete combustion of hydrocarbon fuels. CO emissions are reduced by the presence of hydrogen gas in the gasoline engine. The injection of 3% H_2, 6% H_2, and 9% H_2 of hydrogen gas caused a reduction of 3.5%, 6.9%, and 10.9% in CO emissions compared to pure gasoline. This can be attributed mainly to the high speed of the flame and the high temperatures, which promote the oxidation of CO to CO_2 molecules.

Figure 8 shows the carbon dioxide emissions for the different fuel mixes and engine load percentages.

In general, CO_2 emissions are observed to increase in engine load due to increased fuel injection and high temperature inside the combustion chamber, which promotes complete combustion. On the other hand, the increase in the percentage of hydrogen in gasoline causes a

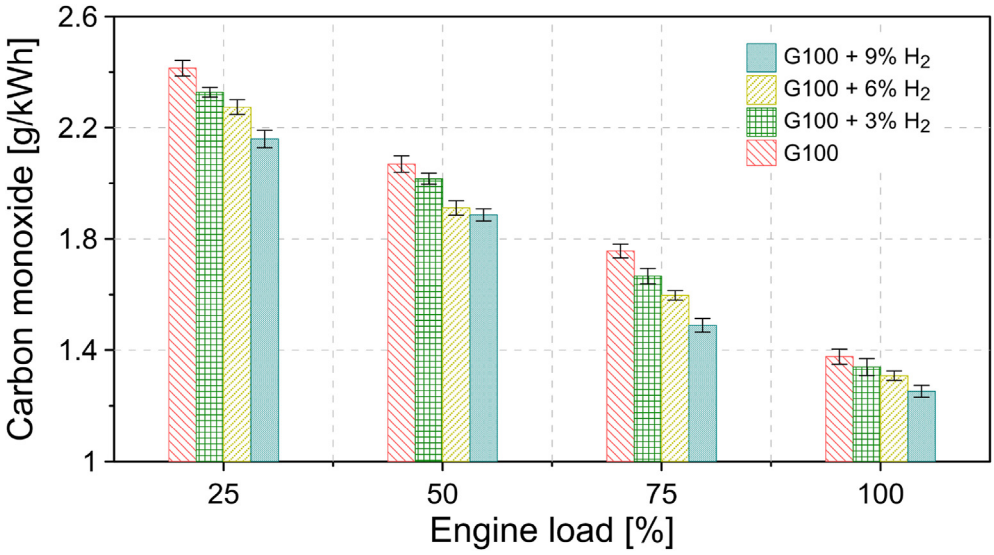

Figure 7. Carbon monoxide emissions for different load conditions.

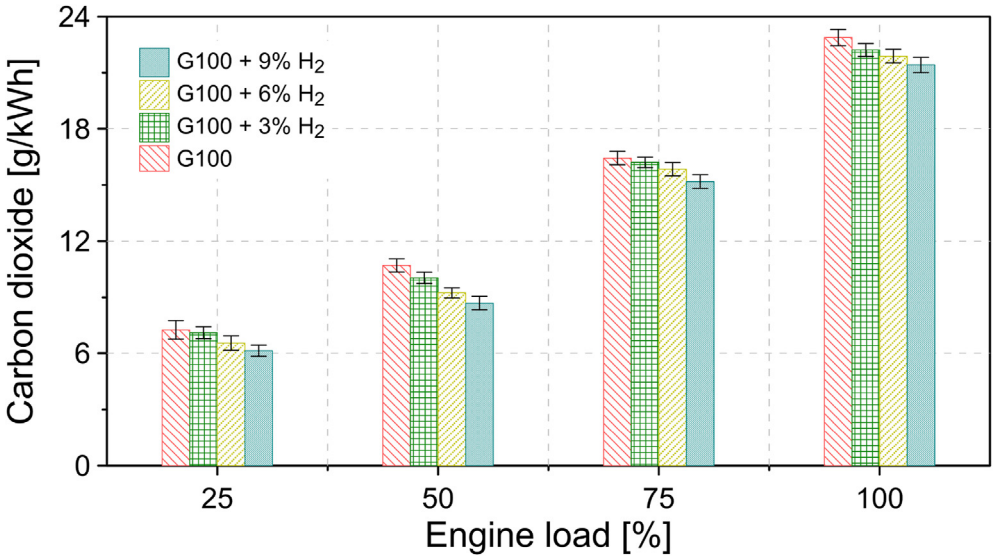

Figure 8. Carbon dioxide emissions for different load conditions.

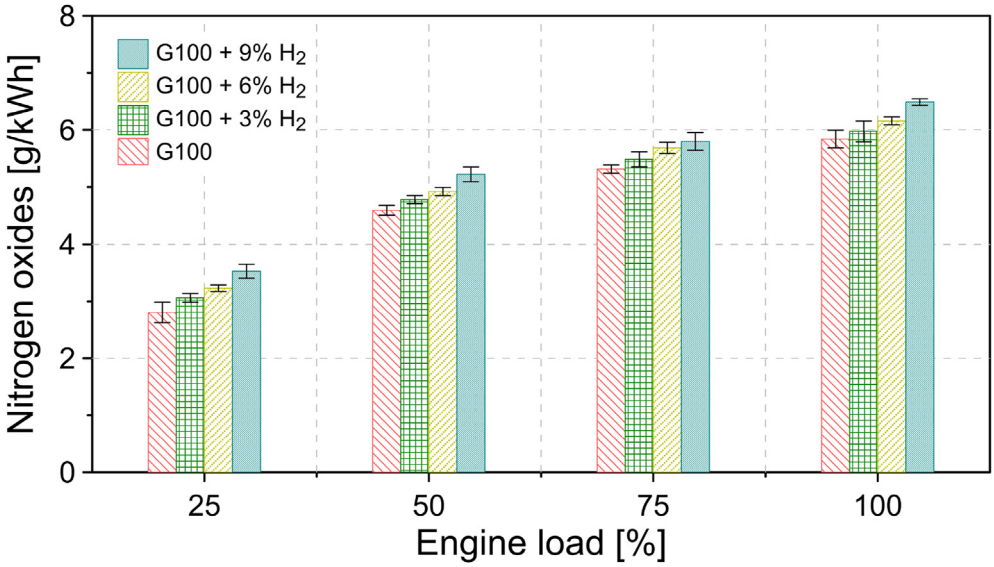

Figure 9. Nitrogen oxides emissions for different load conditions.

reduction in CO_2 emissions. On average, the enrichment of 3%, 6%, and 9% of hydrogen allows a decrease of 3.1%, 7.8%, and 12.1% in CO_2 emissions compared to gasoline. The reduction in CO_2 emissions with the addition of hydrogen gas can be attributed to the absence of carbon atoms in this type of fuel. Similar results are reported in the literature [5, 54].

Figure 9 describes the formation of nitrogen oxides (NOx) for the different gasoline mixtures with hydrogen gas.

The formation of NOx is associated with the oxidation of nitrogenous, which arises from high combustion temperatures and oxygen concentration. This is due to high-temperature conditions dissociating oxygen molecules and reacting with nitrogen to form NOx [55]. The results indicated an increase in NOx emissions with the addition of hydrogen. This is directly associated with the increase in the temperature of the adiabatic flame and the delay in the start of combustion, which leads to a greater accumulation of fuel. From the mixtures G100 + 3% H_2, G100 + 6% H_2 and G100 + 9% H_2, an increase of 4.7%, 8.7% and 14.9% in NOx emissions was observed compared to pure fuel.

For the lowest load condition (25%), NOx emissions of 2.80 g/kWh, 3.06 g/kWh, 3.23 g/kWh and 3.53 g/kWh were observed in fuels G100 + 3% H_2, G100 + 6% H_2 and G100 + 9% H_2, respectively. However, for the highest load condition (100%), NOx levels of 5.84 g/kWh, 5.98 g/kWh, 6.16 g/kWh, and 6.49 g/kWh were obtained. The increase in engine load leads to an increase in NOx emissions from the engine for all fuels. This result is related to the increase in temperature with higher load conditions, which facilitates the stoichiometric mixture for the formation of NOx.

The change in hydrocarbon (HC) emissions as a function of engine load and different combustion conditions are shown in Figure 10.

The results in Figure 10 indicated that the highest levels of HC emissions occur in pure gasoline. In general, it was observed that the addition of hydrogen favors the reduction of HC levels. This is due to the fact that hydrogen is not a hydrocarbon fuel. Therefore, it is free of carbon molecules. This caused a reduction in the rate of HC production due to the reduction in the C/H ratio [56]. On the other hand, the high adiabatic velocity of the hydrogen flame and its high temperature led to improved combustion, leads to a higher fuel burning, and, therefore, a reduction in HC levels [57]. The addition of 3% H_2, 6% H_2, and 9% H_2 of hydrogen gas allows a decrease of 3.3%, 6.7%, and 9.8% compared to pure gasoline.

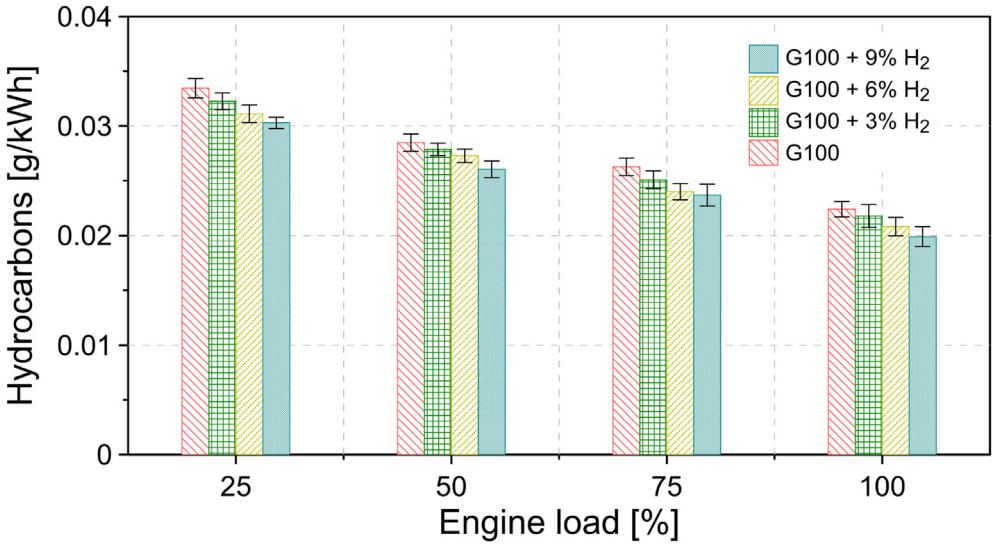

Figure 10. Hydrocarbons emissions for different load conditions.

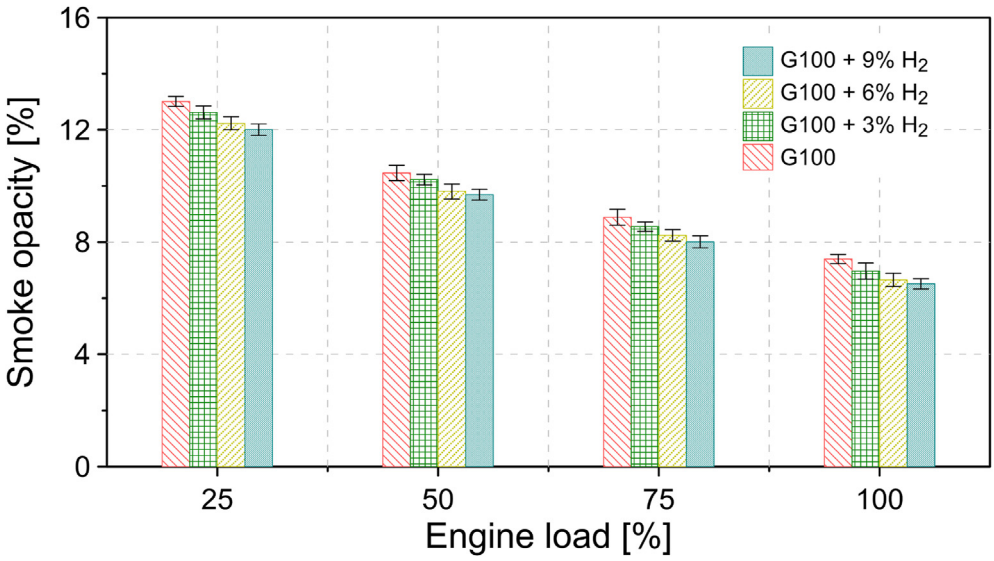

Figure 11. Smoke opacity for different load conditions.

Figure 11 shows the smoke opacity of the engine at different load conditions.

The opacity in the exhaust gases results from the carbonaceous materials produced during the combustion process. This type of material is made up of particles that could not mix adequately with oxygen and, therefore, remained unburned. The results of Figure 11 indicated that the addition of hydrogen gas in gasoline reduces the percentages of smoke opacity. This is a consequence of a better combustion process, which facilitates the oxidation of soot particles. Another factor contributing to the decrease in smoke opacity is the absence of carbon molecules in the hydrogen. For a 100% load on the engine, a percentage of smoke opacity of 7.4%, 7.0%, 6.6% and 6.5% was evidenced in fuels G100, G100 + 3% H_2, G100 + 6% H_2 and G100 + 9% H_2, respectively. In general, the increase in engine load causes a decrease in smoke opacity, which may be related to the high temperature and pressure conditions that facilitate the oxidation of particulate matter.

4.4. Characteristics of lubricating oil

To analyze the changes in the lubrication characteristics, with hydrogen gas in the gasoline engine, the properties of kinematic viscosity, total base number (TBN), total acid number (TAN), and wear debris in the lubricating oil were evaluated.

The variation of the kinematic viscosity of the lubricating oil for a temperature of 40 °C and 100 °C are indicated in Figures 12(a, b).

Lubricating oil viscosity is a measure of the fluid's internal resistance to flow at a particular temperature. Viscosity is considered one of the main parameters to study the condition of lubricating oil. This is due to its important role in maintaining a film thickness between the piston and cylinder liner. Due to the above, changes in viscosity lead to adverse effects on engine lubrication. These changes may be related to oxidation, additive depletion, dilution, and vaporization of lighter compounds.

The initial kinematic viscosity of the lubricating oil is 105.4 cSt and 14.18 cSt for a temperature of 40 °C and 100 °C. This property is indicative of thickening, increased levels of contamination, and insolubility. The reduction in viscosity implies a dilution and shearing of the lubricant. During the operation of the engine with pure gasoline, the kinematic viscosity was reduced by 26.3% (77.59 cSt) and 23.9% (10.8 cSt) for a temperature of 40 °C and 100 °C. However, with the addition of 3% H_2, 6% H_2, and 9% H_2 of hydrogen gas, a reduction of 27.6% (74.29 cSt), 30.8% (71.58 cSt), and 35.7% (67.52 cSt) was observed for a temperature of 40 °C, and 25.4% (10.4 cSt), 27.6% (10.2 cSt) and 29.1%

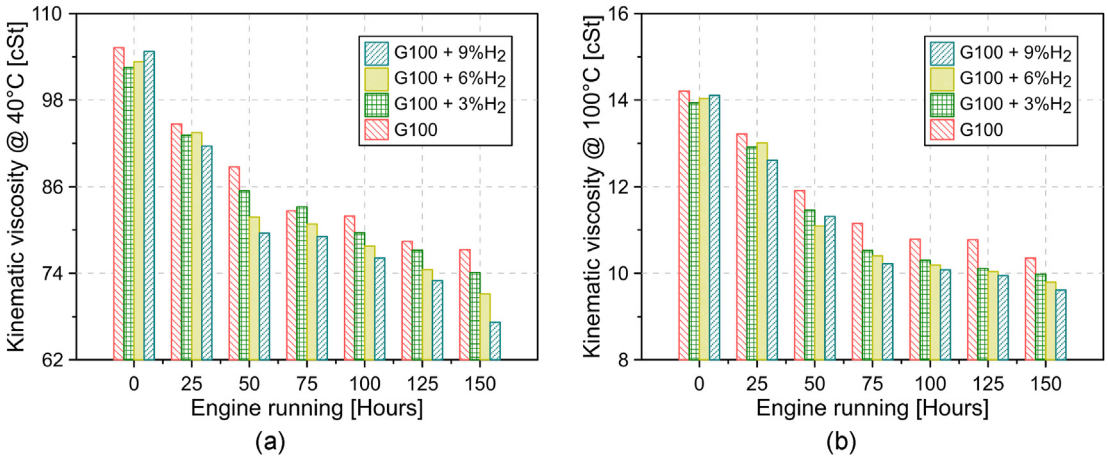

Figure 12. Variation of the kinematic viscosity for a temperature of (a) 40 °C and (b) 100 °C.

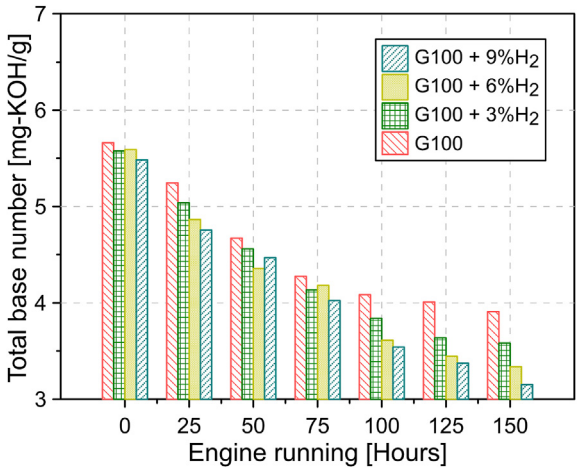

Figure 13. Variation of the total base number.

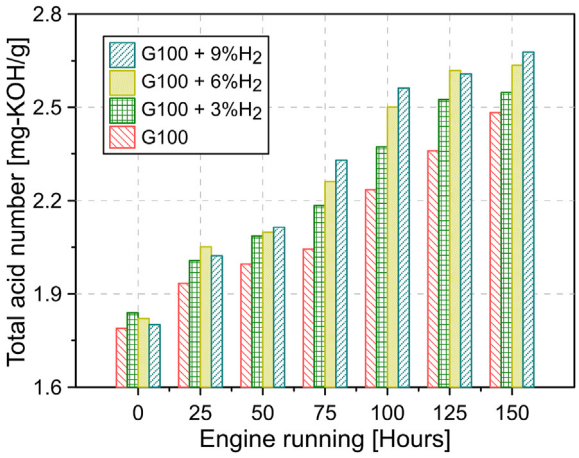

Figure 14. Variation of the total acid number.

(10 cSt) for a temperature of 100 °C, respectively. This implies a greater thermal shear of the lubricating oil. This result is associated with higher temperature in the combustion chamber with the addition of hydrogen gas. Similar results are reported in the literature [31].

Figure 13 depicts the total base number (TBN) variation in lubricating oil.

The TBN is an indication of the alkalinity of the lubricating oil. TBN measures the lubricant's ability to neutralize corrosive acids that form during engine operation. The reduction of this parameter implies a decrease in the resistance of the acids formed during the combustion cycles. This implies a depletion of anti-corrosion additives and greater contamination of the lubricating oil, which weakens the protection of engine components against corrosion. The results showed a decrease of 29.4% (4.0 mg-KOH/g) in the engine operating with pure gasoline's TBN. However, the addition of 3% H_2, 6% H_2, and 9% H_2 hydrogen gas led to a reduction of 35.7% (3.6 mg-KOH/g), 39.2% (3.4 mg-KOH/g), and 40.1% (3.35 mg-KOH/g) in the TBN of the lubricating oil.

Total acid number (TAN) is a parameter that represents the acidity present in engine lubricating oil. The change in TAN for the different hydrogen gas addition conditions is shown in Figure 14.

The TAN is a primary indicator of lubricating oil acidity, which tends to increase due to corrosion and oxidation. Therefore, it is a key indicator to quantify lubricating oil degradation and identify when replacement is necessary. In general, it was evidenced that the hydrogen gas in the combustion chamber increased TAN, which implies more significant oxidation and contamination of the lubricating oil. This result can be a consequence of the increased formation of nitrogen oxides and the high combustion temperatures. It was observed that the addition of 3% H_2, 6% H_2, and 9% H_2 of hydrogen gas produces an increase of 38.5% (2.55 mg-KOH/g), 44.2% (2.62 mg-KOH/g), and 48.6% (2.68 mg-KOH/g) in the TAN of the lubricating oil. Similar results are reported in the literature [29].

To analyze the wear debris in the lubricating oil, a spectrochemical analysis was performed. The variation in the composition of Fe and Cu in the oil is described in Figure 15(a,b).

Figure 15 shows a considerable increase in the presence of Fe and Cu in the lubricating oil with the injection of hydrogen gas in the combustion chamber. It was observed that the mixtures G100 + 3% H_2, G100 + 6% H_2 and G100 + 9% H_2 cause an increase of 22.5% (55.11 ppm), 28.9% (58.0 ppm) and 34.2% (60.39 ppm) in the presence of Fe compared to pure gasoline. In the case of Cu, increases of 30.3% (17.19 ppm), 42.5% (18.81 ppm), and 51.5% (20.0 ppm) were evidenced. The trends described above can be attributed to the decrease in the viscosity of the lubricating oil when the engine operates with hydrogen gas since this causes a decrease in the lubricant film between the cylinder liner and the rings well as in the engine bearings. This results in the detachment of materials in the piston rings, cylinder liners, and bearings, which are manufactured from iron and copper alloys. The presence of this wear debris in the lubricant implies an acceleration in the wear of the engine's internal components. Similar results are reported in the literature [28].

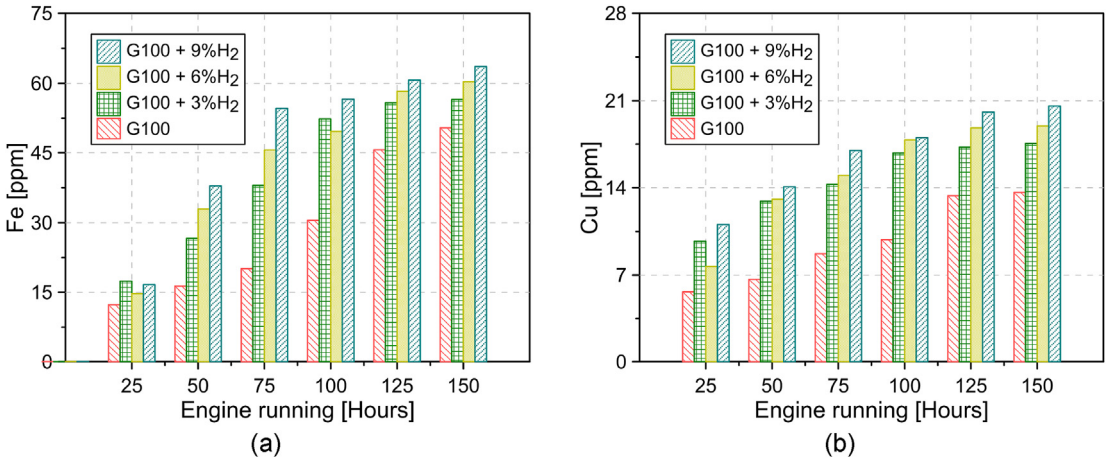

Figure 15. Variations in wear debris of the lubricating oil (a) Fe and (b) Cu.

5. Conclusions

In the present investigation, an analysis of the effect of the injection of hydrogen gas on a spark-ignition engine fueled with gasoline was carried out. The study involved the evaluation of the combustion characteristics, performance parameters, emissions, and changes in the physicochemical characteristics of the lubricating oil.

The results evidenced that the injection of hydrogen gas in pure gasoline increases the maximum combustion pressure levels and increases the heat release rates. In general, an increase of 3.2% and 4.0% in the previous combustion characteristics was evidenced, which implies an improvement in the combustion process compared to pure gasoline.

The high calorific power and the high degree of flammability of hydrogen gas allow for improving engine performance parameters, such as brake specific fuel consumption and brake thermal efficiency. This is the cause of reducing the consumption of fossil fuels such as gasoline. In general, a 1.2% reduction in BSFC and a 2.9% increase in engine BTE were demonstrated.

The improvement in the combustion process and the absence of carbon molecules in the hydrogen gas allow a reduction of 7.1%, 3.9%, 6.6%, and 9.5% in CO, CO_2, HC, and smoke opacity emissions in the engine, compared to pure gasoline. However, high combustion temperatures favor the formation of NOx.

It was shown that the gasoline-hydrogen gas mixture caused an increase of 14.5% in the reduction of the kinematic viscosity. The increase in combustion temperature and the more significant presence of NOx produces a 14.6% increase in the total acid number of the oil concerning pure gasoline. Additionally, there was an increase of 38.3% in the total base number of lubricating oils compared to pure gasoline.

Another disadvantage of the addition of hydrogen gas in gasoline engines is the increased concentration of wear debris, such as Fe and Cu, which implies a greater risk of wear in the engine's internal components.

In future research, the study of metal concentrations and the effect of additives in lubricating oil when the engine operates on gasoline-hydrogen gas mixtures will be expanded.

Declarations

Author contribution statement

Carlos Pardo García: Conceived and designed the experiments; Performed the experiments; Wrote the paper.

Sofia Orjuela Abril: Performed the experiments; Analyzed and interpreted the data; Wrote the paper.

Jhon Pabón León: Contributed reagents, materials, analysis tools or data; Wrote the paper.

Funding statement

This work was supported by Universidad Francisco de Paula Santander.

Data availability statement

Data included in article/supp. material/referenced in article.

Declaration of interest's statement

The authors declare no conflict of interest.

Additional information

No additional information is available for this paper.

Acknowledgements

The authors would like to acknowledge the Universidad Francisco de Paula Santander for their support in the development of this investigation.

References

[1] B. Alhayani, A.A. Abdallah, Manufacturing intelligent Corvus corone module for a secured two way image transmission under WSN, Eng. Comput. (2020).
[2] P. Jakliński, J. Czarnigowski, An experimental investigation of the impact of added HHO gas on automotive emissions under idle conditions, Int. J. Hydrogen Energy 45 (2020) 13119–13128.
[3] M. Usman, N. Hayat, Lubrication, emissions, and performance analyses of LPG and petrol in a motorbike engine: A comparative study, J. Chinese Inst. Eng. 43 (2020) 47–57.
[4] F. Salek, M. Babaie, A. Ghodsi, S.V. Hosseini, A. Zare, Energy and exergy analysis of a novel turbo-compounding system for supercharging and mild hybridization of a gasoline engine, J. Therm. Anal. Calorim. 145 (2021) 817–828.
[5] P. Sharma, A. Dhar, Effect of hydrogen supplementation on engine performance and emissions, Int. J. Hydrogen Energy. 43 (2018) 7570–7580.
[6] X. Yu, H. Wu, Y. Du, Y. Tang, L. Liu, R. Niu, Research on cycle-by-cycle variations of an SI engine with hydrogen direct injection under lean burn conditions, Appl. Therm. Eng. 109 (2016) 569–581.
[7] G. Li, X. Yu, Z. Jin, Z. Shang, D. Li, Y. Li, Z. Zhao, Study on effects of split injection proportion on hydrogen mixture distribution, combustion and emissions of a gasoline/hydrogen SI engine with split hydrogen direct injection under lean burn condition, Fuel 270 (2020), 117488.
[8] J. Wang, X. Duan, Y. Liu, W. Wang, J. Liu, M.-C. Lai, Y. Li, G. Guo, Numerical investigation of water injection quantity and water injection timing on the thermodynamics, combustion and emissions in a hydrogen enriched lean-burn natural gas SI engine, Int. J. Hydrogen Energy. 45 (2020) 17935–17952.
[9] C. Park, C. Kim, S. Lee, S. Lee, J. Lee, Comparative evaluation of performance and emissions of CNG engine for heavy-duty vehicles fueled with various caloric natural gases, Energy 174 (2019) 1–9.

[10] J. Alexander, E. Porpatham, Investigations on combustion characteristics of lean burn SI engine fuelled with Ethanol and LPG, in: IOP Conf. Ser. Earth Environ. Sci., 2019, 12020.
[11] M. Rahman, others, Induction of hydrogen, hydroxy, and LPG with ethanol in a common SI engine: a comparison of performance and emission characteristics, Environ. Sci. Pollut. Res. 26 (2019) 3033–3040.
[12] A.A. Yontar, Y. Do\ugu, Effects of equivalence ratio and CNG addition on engine performance and emissions in a dual sequential ignition engine, Int. J. Engine Res. 21 (2020) 1067–1082.
[13] J. Liu, C.E. Dumitrescu, Flame development analysis in a diesel optical engine converted to spark ignition natural gas operation, Appl. Energy. 230 (2018) 1205–1217.
[14] H.A. Alrazen, K.A. Ahmad, HCNG fueled spark-ignition (SI) engine with its effects on performance and emissions, Renew. Sustain. Energy Rev. 82 (2018) 324–342.
[15] R. Amirante, E. Distaso, S. Di Iorio, P. Sementa, P. Tamburrano, B.M. Vaglieco, R.D. Reitz, Effects of natural gas composition on performance and regulated, greenhouse gas and particulate emissions in spark-ignition engines, Energy Convers. Manag. 143 (2017) 338–347.
[16] J.B. Greenwood, P.A. Erickson, J. Hwang, E.A. Jordan, Experimental results of hydrogen enrichment of ethanol in an ultra-lean internal combustion engine, Int. J. Hydrogen Energy 39 (2014) 12980–12990.
[17] S.J. Nikhil Aniruddha Bhave, Mahendra Gupta, Analysis of performance, emissions, and lubrication in a spark-2 ignition engine fueled with hydrogen gas mixtures, in: SAE Pap, 2021.
[18] B. Subramanian, S. Ismail, Production and use of HHO gas in IC engines, Int. J. Hydrogen Energy 43 (2018) 7140–7154.
[19] M.M. El-Kassaby, Y.A. Eldrainy, M.E. Khidr, K.I. Khidr, Effect of hydroxy (HHO) gas addition on gasoline engine performance and emissions, Alexandria Eng. J. 55 (2016) 243–251.
[20] N. Castro, M. Toledo, G. Amador, An experimental investigation of the performance and emissions of a hydrogen-diesel dual fuel compression ignition internal combustion engine, Appl. Therm. Eng. 156 (2019) 660–667.
[21] Y. Karagöz, Ö. Balcı, E. Orak, M.S. Habib, Effect of hydrogen addition using on-board alkaline electrolyser on SI engine emissions and combustion, Int. J. Hydrogen Energy 43 (2018) 11275–11285.
[22] W. Tutak, A. Jamrozik, K. Grab-Rogaliński, Effect of natural gas enrichment with hydrogen on combustion process and emission characteristic of a dual fuel diesel engine, Int. J. Hydrogen Energy. 45 (2020) 9088–9097.
[23] M. Ebrahimi, S.A. Jazayeri, Effect of hydrogen addition on RCCI combustion of a heavy duty diesel engine fueled with landfill gas and diesel oil, Int. J. Hydrogen Energy 44 (2019) 7607–7615.
[24] J. Zareei, M. Haseeb, K. Ghadamkheir, S.A. Farkhondeh, A. Yazdani, K. Ershov, The effect of hydrogen addition to compressed natural gas on performance and emissions of a DI diesel engine by a numerical study, Int. J. Hydrogen Energy 45 (2020) 34241–34253.
[25] A. Dhar, A.K. Agarwal, Experimental investigations of effect of Karanja biodiesel on tribological properties of lubricating oil in a compression ignition engine, Fuel 130 (2014) 112–119.
[26] A. Sharma, S. Murugan, Durability analysis of a single cylinder DI diesel engine operating with a non-petroleum fuel, Fuel 191 (2017) 393–402.
[27] A. Zare, T.A. Bodisco, M. Jafari, P. Verma, L. Yang, M. Babaie, M.M. Rahman, A. Banks, Z.D. Ristovski, R.J. Brown, et al., Cold-start NOx emissions: diesel and waste lubricating oil as a fuel additive, Fuel 286 (2021), 119430.
[28] S.K. Asrar Hussain, M. Usman, J. Umer, M. Farooq, F. Noor, R. Anjum, A novel analysis of n-butanol–gasoline blends impact on spark ignition engine characteristics and lubricant oil degradation, Energy Sources, Part A Recover. Util. Environ. Eff. (2022) 1–15.
[29] M. Usman, N. Hayat, M.M.A. Bhutta, SI engine fueled with gasoline, CNG and CNG-HHO blend: comparative evaluation of performance, emission and lubrication oil deterioration, J. Therm. Sci. 30 (2021) 1199–1211.
[30] F. Yan, L. Xu, Y. Wang, Application of hydrogen enriched natural gas in spark ignition IC engines: from fundamental fuel properties to engine performances and emissions, Renew. Sustain. Energy Rev. 82 (2018) 1457–1488.
[31] M. Usman, M.W. Saleem, S. Saqib, J. Umer, A. Naveed, Z.U. Hassan, SI engine performance, lubricant oil deterioration, and emission: a comparison of liquid and gaseous fuel, Adv. Mech. Eng. 12 (2020), 1687814020930451.
[32] R. Mathai, R.K. Malhotra, K.A. Subramanian, L.M. Das, Comparative evaluation of performance, emission, lubricant and deposit characteristics of spark ignition engine fueled with CNG and 18% hydrogen-CNG, Int. J. Hydrogen Energy 37 (2012) 6893–6900.
[33] M. Usman, S. Saqib, S.W.H. Zubair, M. Irshad, A.H. Kazmi, A. Noor, H.U. Zaman, Z. Nasir, M.A. Ijaz Malik, Experimental assessment of regenerated lube oil in spark-ignition engine for sustainable environment, Adv. Mech. Eng. 12 (2020), 1687814020940451.
[34] A.E. Eman, A.M. Shoaib, Re-refining of used lube oil, II-by solvent/clay and acid/clay-percolation processes, ARPN J. Sci. Technol. 2 (2012) 1034–1041.
[35] P. Mousavi, D. Wang, C.S. Grant, W. Oxenham, P.J. Hauser, Effects of antioxidants on the thermal degradation of a polyol ester lubricant using GPC, Ind. Eng. Chem. Res. 45 (2006) 15–22.
[36] A.A. Al-Rousan, A. Sa'ed, Effect of anodes-cathodes inter-distances of HHO fuel cell on gasoline engine performance operating by a blend of HHO, Int. J. Hydrogen Energy. 43 (2018) 19213–19221.
[37] A. Boiler, P.V. Code, Section viii division 1, Rules Constr. Press. Vessel. Append. 1, 2010, p. 1.
[38] A.T. Hoang, V.V. Pham, A study of emission characteristic, deposits, and lubrication oil degradation of a diesel engine running on preheated vegetable oil and diesel oil, Energy Sources, Part A Recover, Util. Environ. Eff. 41 (2019) 611–625.
[39] Ü. Agbulut, S. Saridemir, S. Albayrak, Experimental investigation of combustion, performance and emission characteristics of a diesel engine fuelled with diesel–biodiesel–alcohol blends, J. Braz. Soc. Mech. Sci. Eng. 41 (2019) 1–12.
[40] M.J. Moran, G. Tsatsaronis, Engineering thermodynamics, in: CRC Handb. Therm. Eng, second ed., CRC Press, 2017, pp. 1–112.
[41] F. Consuegra, A. Bula, W. Guillín, J. Sánchez, J. Duarte Forero, Instantaneous in-cylinder volume considering deformation and clearance due to lubricating film in reciprocating internal combustion engines, Energies 12 (2019) 1437.
[42] M.S.M. Perera, S. Theodossiades, H. Rahnejat, Elasto-multi-body dynamics of internal combustion engines with tribological conjunctions, Proc. Inst. Mech. Eng. Part K J. Multi-Body Dyn. 224 (2010) 261–277.
[43] L. Estrada, E. Moreno, A. Gonzalez-Quiroga, A. Bula, J. Duarte-Forero, Experimental assessment of performance and emissions for hydrogen-diesel dual fuel operation in a low displacement compression ignition engine, Heliyon 8 (4) (2022), e09285.
[44] J. Duarte-Forero, D. Mendoza-Casseres, G. Valencia-Ochoa, Energy, Exergy, and emissions (3E) assessment of a low-displacement engine powered by biodiesel blends of palm oil mill effluent (POME) and hydroxy gas, Therm. Sci. Eng. Progress 26 (2021), 101126.
[45] M.F. Dabbaghi, M.B. Baharom, Z.A.A. Karim, A.R.A. Aziz, S.E. Mohammed, others, Comparative evaluation of different heat transfer correlations on a single curved-cylinder spark ignition crank-rocker engine, Alexandria Eng. J. 60 (2021) 2963–2978.
[46] J.S. Rosa, G.D. Telli, C.R. Altafini, P.R. Wander, L.A.O. Rocha, Dual fuel ethanol port injection in a compression ignition diesel engine: Technical analysis, environmental behavior, and economic viability, J. Clean. Prod. 308 (2021), 127396.
[47] M. Vergel-Ortega, G. Valencia-Ochoa, J. Duarte-Forero, Experimental study of emissions in single-cylinder diesel engine operating with diesel-biodiesel blends of palm oil-sunflower oil and ethanol, Case Stud. Therm. Eng. 26 (2021), 101190.
[48] G. Zamboni, M. Capobianco, Influence of high and low pressure EGR and VGT control on in-cylinder pressure diagrams and rate of heat release in an automotive turbocharged diesel engine, Appl. Therm. Eng. 51 (2013) 586–596.
[49] Q. Fang, J. Fang, J. Zhuang, Z. Huang, Influences of pilot injection and exhaust gas recirculation (EGR) on combustion and emissions in a HCCI-DI combustion engine, Appl. Therm. Eng. 48 (2012) 97–104.
[50] Z. Wang, G. Du, D. Wang, Y. Xu, M. Shao, Combustion process decoupling of a diesel/natural gas dual-fuel engine at low loads, Fuel 232 (2018) 550–561.
[51] T.S. Hora, A.K. Agarwal, Experimental study of the composition of hydrogen enriched compressed natural gas on engine performance, combustion and emission characteristics, Fuel 160 (2015) 470–478.
[52] S. Sharma, D. Sharma, S.L. Soni, D. Singh, A. Jhalani, Performance, combustion and emission analysis of internal combustion engines fuelled with acetylene–a review, Int. J. Ambient Energy. (2019) 1–19.
[53] E. Arslan, N. Kahraman, The effects of hydrogen enriched natural gas under different engine loads in a diesel engine, Int. J. Hydrogen Energy (2021).
[54] H. Koten, Hydrogen effects on the diesel engine performance and emissions, Int. J. Hydrogen Energy. 43 (2018) 10511–10519.
[55] S. Thiyagarajan, V. Edwin Geo, B. Ashok, K. Nanthagopal, R. Vallinayagam, C.G. Saravanan, P. Kumaran, NOx emission reduction using permanent/electromagnet-based fuel reforming system in a compression ignition engine fueled with pine oil, Clean Technol, Environ. Policy 21 (2019) 815–825.
[56] G. Verma, R.K. Prasad, R.A. Agarwal, S. Jain, A.K. Agarwal, Experimental investigations of combustion, performance and emission characteristics of a hydrogen enriched natural gas fuelled prototype spark ignition engine, Fuel 178 (2016) 209–217.
[57] W.M. Adaileh, K.S. AlQdah, Performance improvement and emission reduction of gasoline engine by adding hydrogen gas into the intake manifold, Mater. Today Proc. (2021).